BASS XXXVII: the role of radiative feedback in the growth and obscuration properties of nearby supermassive black holes

Ricci, C.; Ananna, T.T.; Temple, M.J.; Urry, C.M.; Koss, M.J.; Trakhtenbrot, B.; ... ; Harrison, F.

CrossMark

BASS XXXVII: The Role of Radiative Feedback in the Growth and Obscuration Properties of Nearby Supermassive Black Holes

C. Ricci[1,2], T. T. Ananna[3], M. J. Temple[1], C. M. Urry[4], M. J. Koss[5,6], B. Trakhtenbrot[7], Y. Ueda[8], D. Stern[9], F. E. Bauer[10,11,12], E. Treister[10], G. C. Privon[13,14], K. Oh[15], S. Paltani[16], M. Stalevski[17,18], L. C. Ho[2,19], A. C. Fabian[20], R. Mushotzky[21,22], C. S. Chang[23], F. Ricci[24,25], D. Kakkad[26], L. Sartori[27], R. Baer[27], T. Caglar[28], M. Powell[29], and F. Harrison[30]

[1] Núcleo de Astronomía de la Facultad de Ingeniería, Universidad Diego Portales, Av. Ejército Libertador 441, Santiago, Chile; claudio.ricci@mail.udp.cl
[2] Kavli Institute for Astronomy and Astrophysics, Peking University, Beijing 100871, People's Republic of China
[3] Department of Physics and Astronomy, Dartmouth College, 6127 Wilder Laboratory, Hanover, NH 03755, USA
[4] Yale Center for Astronomy & Astrophysics, Physics Department, P.O. Box 208120, New Haven, CT 06520-8120, USA
[5] Eureka Scientific, 2452 Delmer Street Suite 100, Oakland, CA 94602-3017, USA
[6] Space Science Institute, 4750 Walnut Street, Suite 205, Boulder, CO 80301, USA
[7] School of Physics and Astronomy, Tel Aviv University, Tel Aviv 69978, Israel
[8] Department of Astronomy, Kyoto University, Kyoto 606-8502, Japan
[9] Jet Propulsion Laboratory, California Institute of Technology, 4800 Oak Grove Drive, MS 169-224, Pasadena, CA 91109, USA
[10] Instituto de Astrofísica, Facultad de Física, Pontificia Universidad Católica de Chile, Campus San Joaquin, Av. Vicuña Mackenna 4860, Macul Santiago, 7820436, Chile
[11] Centro de Astroingeniería, Facultad de Física, Pontificia Universidad Católica de Chile, Campus San Joaquin, Av. Vicuña Mackenna 4860, Macul Santiago, 7820436, Chile
[12] Millennium Institute of Astrophysics, Nuncio Monseñor Sótero Sanz 100, of 104, Providencia, Santiago, Chile
[13] National Radio Astronomy Observatory, 520 Edgemont Road, Charlottesville, VA 22903, USA
[14] Department of Astronomy, University of Florida, P.O. Box 112055, Gainesville, FL 32611, USA
[15] Korea Astronomy & Space Science institute, 776, Daedeokdae-ro, Yuseong-gu, Daejeon 34055, Republic of Korea
[16] Department of Astronomy, University of Geneva, ch. d'Écogia 16, CH-1290 Versoix, Switzerland
[17] Astronomical Observatory, Volgina 7, 11060 Belgrade, Serbia
[18] Sterrenkundig Observatorium, Universiteit Ghent, Krijgslaan 281 S9, B-9000 Ghent, Belgium
[19] Department of Astronomy, School of Physics, Peking University, Beijing 100871, People's Republic of China
[20] Institute of Astronomy, Madingley Road, Cambridge CB3 0HA, UK
[21] Department of Astronomy, University of Maryland, College Park, MD 20742, USA
[22] Joint Space-Science Institute, University of Maryland, College Park, MD 20742, USA
[23] Joint ALMA Observatory, Avenida Alonso de Cordova 3107, Vitacura 7630355, Santiago, Chile
[24] Dipartimento di Fisica e Astronomia, Universita di Bologna, via Gobetti 93/2, I-40129 Bologna, Italy
[25] INAF Osservatorio Astronomico di Bologna, via Gobetti 93/3, I-40129 Bologna, Italy
[26] Space Telescope Science Institute, 3700 San Martin Drive, Baltimore, MD 21218, USA
[27] Institute for Astronomy, Department of Physics, ETH Zurich,Wolfgang-Pauli-Strasse 27, CH-8093 Zurich, Switzerland
[28] Leiden Observatory, P.O. Box 9513, 2300 RA, Leiden, The Netherlands
[29] Institute of Particle Astrophysics and Cosmology, Stanford University, 452 Lomita Mall, Stanford, CA 94305, USA
[30] Cahill Center for Astronomy and Astrophysics, California Institute of Technology, Pasadena, CA 91125, USA

Abstract

We study the relation between obscuration and supermassive black hole (SMBH) accretion using a large sample of hard X-ray selected active galactic nuclei (AGNs). We find a strong decrease in the fraction of obscured sources above the Eddington limit for dusty gas ($\log \lambda_{\mathrm{Edd}} \gtrsim -2$) confirming earlier results, and consistent with the radiation-regulated unification model. This also explains the difference in the Eddington ratio distribution functions (ERDFs) of type 1 and type 2 AGNs obtained by a recent study. The break in the ERDF of nearby AGNs is at $\log \lambda_{\mathrm{Edd}}^{*} = -1.34 \pm 0.07$. This corresponds to the λ_{Edd} where AGNs transition from having most of their sky covered by obscuring material to being mostly devoid of absorbing material. A similar trend is observed for the luminosity function, which implies that most of the SMBH growth in the local universe happens when the AGN is covered by a large reservoir of gas and dust. These results could be explained with a radiation-regulated growth model, in which AGNs move in the N_{H}–λ_{Edd} plane during their life cycle. The growth episode starts with the AGN mostly unobscured and accreting at low λ_{Edd}. As the SMBH is further fueled, λ_{Edd}, N_{H} and the covering factor increase, leading the AGN to be preferentially observed as obscured. Once λ_{Edd} reaches the Eddington limit for dusty gas, the covering factor and N_{H} rapidly decrease, leading the AGN to be typically observed as unobscured. As the remaining fuel is depleted, the SMBH goes back into a quiescent phase.

Unified Astronomy Thesaurus concepts: Supermassive black holes (1663); Astrophysical black holes (98); Quasars (1319); High energy astrophysics (739); Active galactic nuclei (16); Seyfert galaxies (1447)

1. Introduction

Supermassive black holes (SMBHs; with masses $M_{BH} \geqslant 10^6 M_\odot$) are found at the center of most massive galaxies (e.g., Kormendy & Richstone 1995), and are thought to gain most of their mass through the accretion of matter from their circumnuclear environment (e.g., Soltan 1982; Yu & Tremaine 2002; Shankar et al. 2004). During the rapid accretion phase, SMBHs can emit a large amount of radiation across the entire electromagnetic spectrum (e.g., Elvis et al. 1994), outshining their host galaxies, and are observed as active galactic nuclei (AGNs). The discovery of correlations between SMBH mass and several properties of their host galaxies, such as the luminosity and mass of the bulge (e.g., Marconi & Hunt 2003; Häring & Rix 2004) and the velocity dispersion (e.g., Ferrarese & Merritt 2000; Gebhardt et al. 2000; Kormendy & Ho 2013), has suggested that AGNs could play an important role in the evolution of galaxies. This is usually associated with a feedback process, in which the energy and radiation produced by the AGN interact with the interstellar medium (ISM) of their host galaxies (e.g., Fabian 2012), directly affecting the star formation process. Both semianalytic models of galaxy formation (e.g., Bower et al. 2006; Croton et al. 2006) and hydrodynamical simulations (e.g., Sijacki et al. 2007; Schaye et al. 2015) have demonstrated the importance of AGN feedback, showing that such a mechanism is necessary to regulate star formation and to explain the high-mass end of the galaxy mass function. This feedback process could be associated with either radiative feedback (for luminous AGNs; e.g., Fabian 2012) or to kinetic feedback (for low-luminosity AGNs; e.g., Weinberger et al. 2017).

About 70% of the luminous[31] AGNs in the local universe are found to be obscured by weakly ionized or neutral gas [$\log(N_H/cm^{-2}) \geqslant 22$; Ricci et al. 2015], which implies that gas and dust typically cover a similar fraction of the sky as seen from the nucleus, assuming simple orientation-based unification (e.g., Antonucci 1993; Urry & Padovani 1995). This obscuring material is thought to be located on circumnuclear scales, and distributed anisotropically around the AGN, leading to the classification of AGNs into type 2 (obscured) and type 1 (unobscured) sources (e.g., Antonucci 1993; Netzer 2015; Ramos Almeida & Ricci 2017; Hickox & Alexander 2018). Optical, UV, and soft X-ray ($<10\,keV$) radiation can be strongly suppressed by line-of-sight obscuration, which leads to a strong bias against detecting heavily obscured sources in these energy bands. In the hard X-rays ($\geqslant 10\,keV$), obscuration is less important due to the lower photoelectric cross section of the obscuring material, which enables recovery of most of the X-ray flux up to $\log(N_H/cm^{-2}) \simeq 23.5$ (e.g., Ricci et al. 2015). Therefore, hard X-ray surveys, such as those carried out by INTEGRAL (e.g., Paltani et al. 2008; Beckmann et al. 2009; Krivonos et al. 2022), Swift/Burst Alert Telescope (BAT; e.g., Markwardt et al. 2005; Tueller et al. 2008; Cusumano et al. 2010; Tueller et al. 2010; Baumgartner et al. 2013; Oh et al. 2018), and NuSTAR (e.g., Alexander et al. 2013; Civano et al. 2015; Mullaney et al. 2015; Harrison et al. 2016; Del Moro et al. 2017; Zappacosta et al. 2018a; Masini et al. 2018), are very well suited to detect and characterize obscured AGNs, particularly at low redshift. The all-sky Swift/BAT survey, in particular, has detected ~ 1100 AGNs in the 14–195 keV band (Oh et al. 2018). X-ray follow-up of BAT-detected sources

showed that a significant fraction ($\sim 20\%$–30%) of local AGNs are obscured by Compton-thick material (CT, $\log(N_H/cm^{-2}) \geqslant 24$; e.g., Burlon et al. 2011; Ricci et al. 2015; Akylas et al. 2016; Marchesi et al. 2018; Torres-Albà et al. 2021; Tanimoto et al. 2022).

The nuclear obscuring material can be significantly affected by the strong radiation emitted by the AGN (e.g., Fabian et al. 2006). This feedback process was originally supported by a decrease of the fraction of obscured sources (f_{obs}) with increasing luminosity. This was first discovered 40 yr ago by Lawrence & Elvis (1982; see also Lawrence 1991), and then confirmed by numerous studies carried out in the optical (e.g., Simpson 2005; Oh et al. 2015) and X-rays (e.g., Steffen et al. 2003; Ueda et al. 2003; Barger et al. 2005; La Franca et al. 2005; Treister & Urry 2006; Hasinger 2008; Winter et al. 2009; Brusa et al. 2010; Ueda et al. 2014). Several works focusing on the IR regime also found evidence of a decrease of the covering factor of the obscurer with increasing luminosity (e.g., Maiolino et al. 2007; Treister et al. 2008; Sazonov et al. 2012; Lusso et al. 2013; Stalevski et al. 2016; Mateos et al. 2017; Ichikawa et al. 2019; Lanz et al. 2019; Toba et al. 2021). Several of these early results may however be affected by inconsistent bolometric corrections (Netzer et al. 2016), and by the fact that they did not take into account the effects of anisotropy and radiative transfer (Stalevski et al. 2016). When this is taken into account, the decrease of the covering factor with the AGN luminosity is reduced or disappears altogether (Netzer et al. 2016; Stalevski et al. 2016). As shown by Burlon et al. (2011) in a study of Swift/BAT AGNs, the relation between the fraction of sources with $\log(N_H/cm^{-2}) = 22 - 24$ and the luminosity is tightly connected to the different X-ray luminosity functions (LFs) of obscured and unobscured AGNs (see also Della Ceca et al. 2008; Buchner et al. 2015; Ananna et al. 2019).

Studying a large number of Swift/BAT AGNs, Ricci et al. (2017a) demonstrated that the main parameter driving the fraction of obscured sources is the Eddington ratio (λ_{Edd}). This was done by showing the existence of a steep decrease of f_{obs} at $\log \lambda_{Edd} \gtrsim -2$, which corresponds to the expected Eddington limit for dusty gas with $\log(N_H/cm^{-2}) \simeq 22$ (e.g., Fabian et al. 2006, 2008, 2009; Ishibashi et al. 2018; see also Hönig & Beckert 2007 and Kawakatu et al. 2020). Ricci et al. (2017a) also showed that, when controlling for λ_{Edd}, the relation between f_{obs} and the AGN luminosity disappears. These results suggested that radiative feedback plays a dominant role in shaping the close environments of SMBHs, and led to the formulation of the radiation-regulated unification model (Ricci et al. 2017a), according to which the likelihood of a source to be observed as obscured is higher at low Eddington ratio ($\lambda_{Edd} \lesssim -1.5$; Figure 4 of Ricci et al. 2017a). At higher Eddington ratios ($\lambda_{Edd} \gtrsim -1.5$) the effect of radiation pressure clears the immediate vicinity of the AGN, possibly giving rise to the polar emission that has been observed in a large fraction of AGNs in the mid-IR (e.g., Tristram et al. 2007; Hönig et al. 2013; López-Gonzaga et al. 2016; Hönig & Kishimoto 2017; Asmus 2019; Alonso-Herrero et al. 2021). The fact that λ_{Edd} is the dominant parameter also points toward most of the obscuring material being located within the sphere of influence of the SMBH (typically $\lesssim 60\,pc$ for the sample of Ricci et al. 2017a), in agreement with recent studies carried out with ALMA (e.g., García-Burillo et al. 2021).

In this work we study the dependence of the fraction of AGNs with a given N_H on the Eddington ratio, investigate the

---

[31] With a 14–150 keV luminosity $\log(L_{14-150}/erg\,s^{-1}) \gtrsim 42.5$.

relation between the AGN Eddington ratio distribution function (ERDF) and the covering factor of the circumnuclear material, and explain these relations with a radiation-regulated model for the growth of SMBHs. We use the second BAT AGN Spectroscopic Survey (BASS) data release (DR2; Koss et al. 2022a) to build a sample that contains ~2 times more Swift/BAT AGNs with black hole mass available with respect to the previous study of Ricci et al. (2017a). The BASS DR2 sample is significantly more complete than the DR1 one, with 100% of measured redshifts and ~98% of black hole masses for unbeamed AGNs outside the Galactic plane. This allows us to study, for the first time, the relation between obscuration and $\lambda_{\rm Edd}$ in different ranges of $N_{\rm H}$. In a companion paper (Ananna et al. 2022a) we will present a complementary analysis of the sample, focusing on the timescales of the different stages of AGN growth. Throughout the paper, we adopt standard cosmological parameters ($H_0 = 70 \ {\rm km \ s^{-1} \ Mpc^{-1}}$, $\Omega_{\rm m} = 0.3$, and $\Omega_{\Lambda} = 0.7$). All fractions are calculated following the Bayesian approach outlined in Cameron (2011), and the uncertainties quoted represent the 16th and 84th quantiles of a binomial distribution.

2. Sample

BAT (Barthelmy et al. 2005) on board the Neil Gehrels Swift Observatory (Gehrels et al. 2004) has been carrying out an all-sky survey in the 14–195 keV band since its launch in November 2004. This has led to the detection of more than 1500 sources (e.g., Barthelmy et al. 2005; Oh et al. 2018), including over 1000 AGNs. BASS[32] has been gathering a large number of optical spectroscopy and ancillary multiwavelength data for BAT-selected AGNs. This includes data in the radio (Baek et al. 2019; Smith et al. 2020), millimeter (Koss et al. 2021; Kawamuro et al. 2022), infrared (Ichikawa et al. 2017; Lamperti et al. 2017; Ichikawa et al. 2019; den Brok et al. 2022; Ricci et al. 2022), optical (Koss et al. 2017), and X-rays (Ricci et al. 2017b). This has led to a number of follow-up studies comparing the X-ray continuum and optical properties of AGNs with their accretion rates (Oh et al. 2017; Trakhtenbrot et al. 2017; Ricci et al. 2018; Rojas et al. 2020; Kakkad et al. 2022). The first BASS data release (Koss et al. 2017) reported black hole masses for 473 AGNs, and X-ray properties for all 838 AGNs from the flux-limited Swift/BAT 70 month sample (Ricci et al. 2017b). The second BASS data release (Koss et al. 2022a) reported black hole masses for 780 AGNs, and increased the total number of AGNs from the Swift/BAT 70 month catalog to 858.

In BASS, black hole masses were obtained using single-epoch broad Balmer line measurements for unobscured AGNs and velocity dispersions for obscured AGNs. Typical systematic uncertainties on $M_{\rm BH}$ are ~0.3–0.5 dex. In this work, we use intrinsic X-ray fluxes and column densities from Ricci et al. (2017b), and black hole masses from BASS DR2. Sources that were found to be unobscured in the X-ray band were assigned $\log(N_{\rm H}/{\rm cm^{-2}}) = 20$ (i.e., an upper limit). To calculate the luminosities, we used the updated distances and redshifts reported in Koss et al. (2022b), which are based on emission line redshifts and redshift-independent distance measurements. Eddington ratios were calculated from the intrinsic X-ray luminosities as in Ricci et al. (2017a). Similarly to what was done in Ricci et al. (2017a), we excluded blazars from our
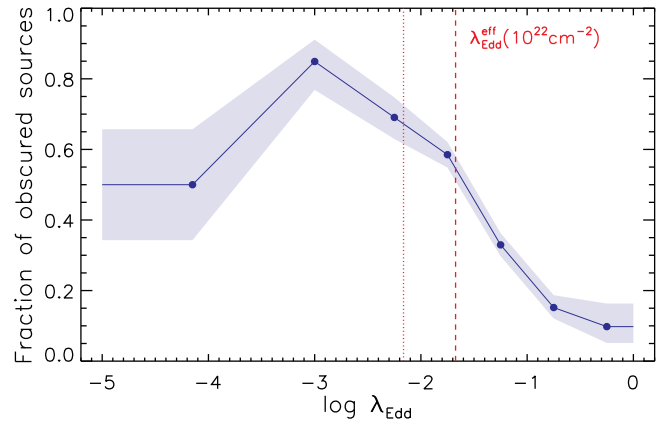
---

[32] www.bass-survey.com

Figure 1. Fraction of obscured Compton-thin [$22 \leqslant \log(N_{\rm H}/{\rm cm^{-2}}) < 24$] sources vs. Eddington ratio for AGNs from our hard X-ray selected sample with $-4.8 \leqslant \log \lambda_{\rm Edd} < 0$. For each $\lambda_{\rm Edd}$ bin, the fractions were normalized to unity in the $20 \leqslant \log(N_{\rm H}/{\rm cm^{-2}}) < 24$ interval. The red lines show the expected Eddington limit for dusty gas with $\log(N_{\rm H}/{\rm cm^{-2}}) \simeq 22$ from Fabian et al. (2006 2008 2009; dashed line) and Ishibashi et al. (2018; dotted line). The fractions are calculated following Cameron (2011), and the uncertainties quoted represent the 16th and 84th quantiles of a binomial distribution.

sample (Paliya et al. 2019) as well as obscured objects for which the black hole mass was estimated using broad optical emission lines, since $M_{\rm BH}$ is typically underestimated for those objects (Mejía-Restrepo et al. 2022). Our final sample consists of 681 AGNs, spanning a large range in 14–150 keV luminosities ($10^{41} - 10^{45.5}$ erg s^{-1}), and with redshifts typically $z < 0.15$ (with most of the objects being located within a few hundred megaparsecs).

3. The Relation between Obscuration and Eddington Ratio

3.1. Obscured Fraction versus Eddington Ratio

Figure 1 shows the relation between the fraction of obscured Compton-thin [$\log(N_{\rm H}/{\rm cm^{-2}}) = 22$–$24$] sources ($f_{\rm obs}$) and the Eddington ratio for our sample. We considered here only sources with $\log(N_{\rm H}/{\rm cm^{-2}}) \leqslant 24$, to maximize the completeness of our selection (see Figure 1 of Ricci et al. 2015). The observed trend reflects what was previously found by Ricci et al. (2017a), with $f_{\rm obs}$ decreasing sharply at $\lambda_{\rm Edd} \gtrsim 10^{-2}$, a value consistent with the expected Eddington limit for dusty gas (red dashed lines; Fabian et al. 2006, 2008, 2009; Ishibashi et al. 2018). Consistent results have been recently obtained using different approaches and samples (see, e.g., She et al. 2018 for a study of nearby low-luminosity AGNs). From careful modeling of the broadband X-ray spectra of nearby AGNs using recently developed torus models, Zhao et al. (2020) and Ogawa et al. (2021) found a decrease of the covering factor of the obscuring material at $\lambda_{\rm Edd} \simeq 10^{-2}$. A decrease of the covering factor with increasing $\lambda_{\rm Edd}$ was also found in the IR (e.g., Ezhikode et al. 2017; Zhuang et al. 2018). This is in agreement with what would be expected by the radiation-regulated unification model (Ricci et al. 2017a), according to which the probability of observing a source as obscured is a function of the inclination angle as well as the Eddington ratio.

Most of the sources in our sample are found to accrete at $\lambda_{\rm Edd} < 1$, with only 10 sources accreting at higher Eddington ratios. Although we have only a small number of sources at $\lambda_{\rm Edd} \geqslant 1$, it is interesting to notice that three of them (LEDA 97012, ESO 383−18, and IRAS 04210+0400) are obscured, which corresponds to $f_{\rm obs} = 32^{+14}_{-12}\%$, a value

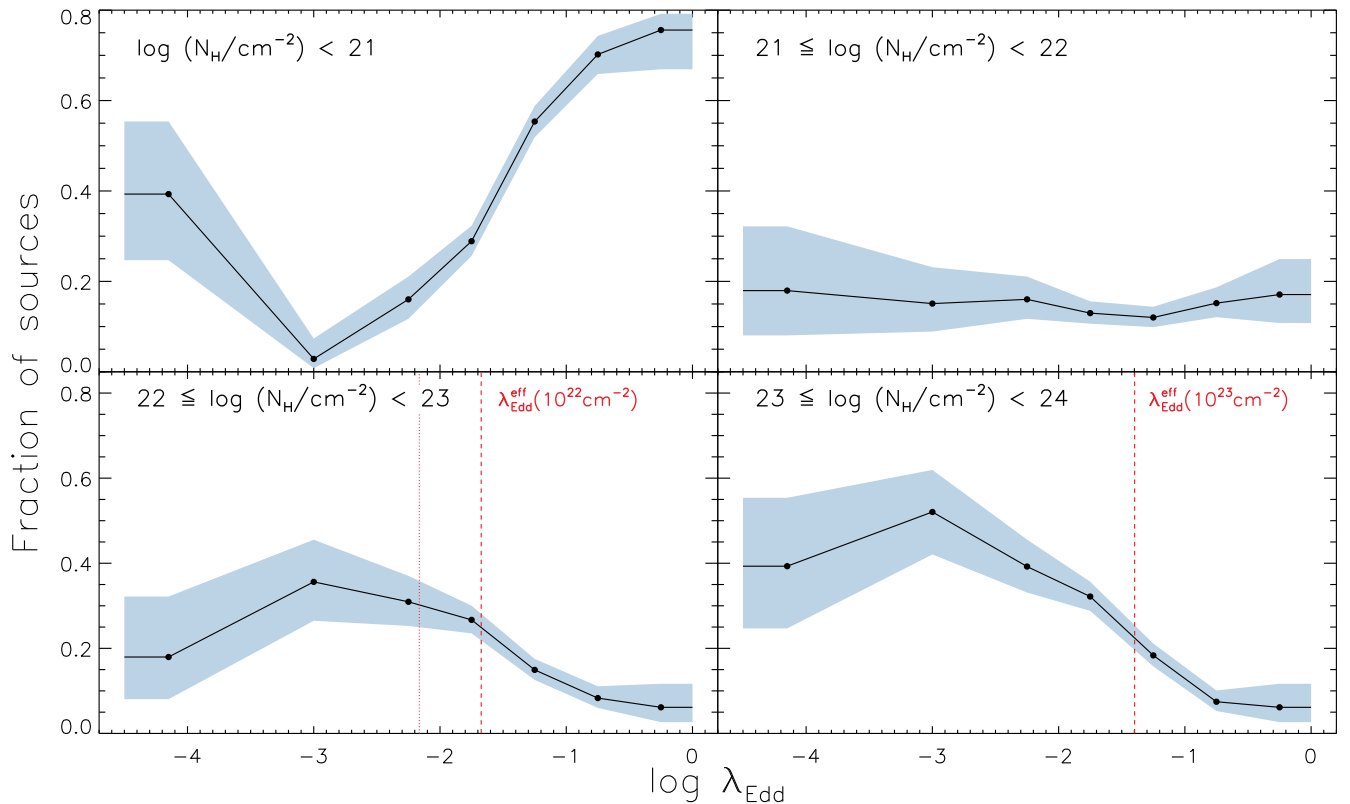**Figure 2.** Fraction of sources with N_H in a given range vs. Eddington ratio for the objects in our hard X-ray selected sample with $-4.5 \leqslant \log \lambda_{Edd} < 0$. For each λ_{Edd} bin, the fractions were normalized to unity in the $20 \leqslant \log(N_H/cm^{-2}) < 24$ interval. The red lines show the expected Eddington limit for dusty gas with $\log(N_H/cm^{-2}) \simeq 22$ (bottom-left panel; dashed line from Fabian et al. 2006, 2008, 2009; dotted line from Ishibashi et al. 2018) and $\log(N_H/cm^{-2}) \simeq 23$ (bottom-right panel; Ishibashi et al. 2018; Venanzi et al. 2020). The latter value of the effective Eddington limit includes the contribution from IR radiation trapping. The fractions are calculated following Cameron (2011), and the uncertainties quoted represent the 16th and 84th quantiles of a binomial distribution.

significantly higher than what we found at $\lambda_{Edd} \simeq 10^{-0.25}$ (see Figure 1). Among these objects, LEDA 97012 is in a merging system (e.g., Koss et al. 2012), ESO 383−18 shows peculiar absorption properties, possibly associated with partial covering (Ricci et al. 2010), while IRAS 04210+0400 shows a relatively high star formation rate (e.g., Ichikawa et al. 2017). Larger studies of nearby AGNs accreting at high Eddington ratios are needed to confirm an increase in f_{obs} at $\lambda_{Edd} \gtrsim 1$.

3.2. $f_{obs}(N_H)$ versus λ_{Edd}

Considering the large number of AGNs with careful measurements of black hole masses provided by BASS DR2 (Koss et al. 2022a, 2022c), we can now explore the trend between the fraction of sources in relatively narrow ranges of N_H and the Eddington ratio. Figure 2 shows that the fraction of sources that show little to no absorption [$\log(N_H/cm^{-2}) < 21$] increases with λ_{Edd}, and that such an increase is particularly steep at $\lambda_{Edd} \gtrsim 10^{-2}$ (top-left panel), in agreement with the idea that radiation pressure is able to clean up the obscuring material very rapidly, leaving most of the sky around the AGN with little or no absorbing material (Ricci et al. 2017a). A similar trend is obtained when selecting only sources with $20 < \log(N_H/cm^{-2}) < 21$. Interestingly, such a trend is not observed for sources with $\log(N_H/cm^{-2}) = 21–22$ (top-right panel), which exhibit a constant fraction of $\simeq 20\%$ across four orders of magnitude in λ_{Edd}. This could be due to the fact that most of the obscuring material in this range of column densities is associated with gas from the host galaxy (e.g., Buchner et al. 2017; Malizia et al. 2020), and therefore is not affected by radiation pressure. In the $\log(N_H/cm^{-2}) = 22–23$ range (bottom-left

panel), we observe a trend that is in good agreement with what is expected by considering the effect of radiation pressure, with a rapid decline at $\lambda_{Edd} \simeq 10^{-2}$. Interestingly, the fraction of sources with $\log(N_H/cm^{-2}) = 23–24$ (bottom-right panel) shows a very similar trend to that of sources with $\log(N_H/cm^{-2}) = 22–23$, with a rapid drop in the fraction of sources with Eddington ratios above a few percent. The Eddington limit for dusty gas is however expected to increase with the column density of the material, and it should be $\lambda_{Edd} \simeq 10^{-1.15}$ for $\log(N_H/cm^{-2}) \simeq 23$ (e.g., Fabian et al. 2006). Recent theoretical studies (e.g., Ishibashi et al. 2018; Venanzi et al. 2020) have shown that infrared radiation trapping could play an important role in the obscuring material, and would allow AGNs to expel dense [$\log(N_H/cm^{-2}) \geqslant 23$] gas at relatively low Eddington ratios ($\lambda_{Edd} \simeq 0.04$), which could explain our new observational results (dashed red vertical line in the bottom-right panel of Figure 2). We explored the same trends of Figure 2 by dividing our sample into different bins of intrinsic 14–150 keV luminosity and black hole mass in Appendix (see Figure 6), and found that these parameters do not appear to have any significant effect on the relation between the fraction of sources with a given N_H and λ_{Edd}.

4. Radiation-regulated Growth of Supermassive Black Holes

4.1. Luminosity and Eddington Ratio Distribution Functions of Nearby AGNs

Luminosity and Eddington ratio distribution functions (ERDFs) can provide important insights on the lifetime of the

different phases of SMBH growth. While AGN LFs have been studied in detail in different bands and at various redshifts (e.g., Ueda et al. [2003]; Nagar et al. [2005]; Caputi et al. [2007]; Hopkins et al. [2007]; Paltani et al. [2008]; Aird et al. [2010]; Ross et al. [2013]; Ueda et al. [2014]; Buchner et al. [2015]), studies of the ERDF (e.g., Kollmeier et al. [2006]; Greene & Ho [2007]; Aird et al. [2012]; Kelly & Shen [2013]; Caplar et al. [2015]; Schulze et al. [2015]; Bongiorno et al. [2016]; Weigel et al. [2017]; Ananna et al. [2022b]) are still relatively scarce. Early efforts to study the ERDF were based on high-luminosity AGNs at $z < 0.3$ from the Hamburg/ESO Survey (Schulze & Wisotzki [2010]), and on $1 < z < 2$ AGNs from different optical surveys (Schulze et al. [2015]). However, these samples were focused on unobscured, high-luminosity AGNs and did not provide a full picture of the SMBH growth. Some other studies have used the stellar mass as an indicator of the black hole mass, and derived ERDFs including for lower-luminosity, obscured systems (e.g., Georgakakis et al. [2017]; Aird et al. [2018]). Recently, studying nearby hard X-ray selected AGNs from BASS, Ananna et al. ([2022b]) calculated the ERDFs of AGNs in the local universe in the $10^{-3} < \lambda_{\rm Edd} < 1$ range for both type 1 and type 2 AGNs (top panel of Figure [3]), finding that the shape of the ERDF is independent of the AGN black hole mass. Ananna et al. ([2022b]) found that the total ERDF can be well reproduced by a double power law with a break at $\log \lambda^*_{\rm Edd} = -1.34 \pm 0.07$. A similar value was inferred by Weigel et al. ([2017]), who proposed that the growth of radiatively efficient (i.e., X-ray detected) and inefficient (i.e., radio detected) AGNs could each have universal ERDFs, which can reproduce both the black hole mass function and the AGN LF. Weigel et al. ([2017]) found that the ERDF of local, radiatively efficient AGNs has a break between $\log \lambda^*_{\rm Edd} = -1.57$ and $\log \lambda^*_{\rm Edd} = -1.11$.

As expected, the ratio between the ERDF of type 2 AGNs and that of the whole AGN population (bottom panel of Figure [3]) shows a similar trend to that observed for the $f_{\rm obs} - \lambda_{\rm Edd}$ relation (Ricci et al. [2017a]). The break in the ERDF of local type 2 AGNs ($\log \lambda^*_{\rm Edd} = -1.66^{+0.09}_{-0.06}$) found by Ananna et al. ([2022b]) is consistent with the Eddington limit for dusty gas, while that of type 1 AGNs is found at higher Eddington ratios ($\log \lambda^*_{\rm Edd} = -1.15^{+0.09}_{-0.05}$). Considering the strong anisotropy of the radiation produced in the accretion disk (e.g., Kawaguchi & Mori [2010]), it is possible that this value is associated with the action of infrared radiation trapping in the optically thick material located along the plane of the accretion disk, which was not blown away at $\log \lambda_{\rm Edd} \sim -2$.

4.2. A Radiation-regulated Model for the Growth of Nearby SMBHs

The value of $\lambda^*_{\rm Edd}$ inferred by Ananna et al. ([2022b]) for the whole AGN population lies in the range at which we find that BASS AGNs transition from being mostly obscured ($f_{\rm obs} > 50\%$) to mostly unobscured ($f_{\rm obs} < 50\%$), as illustrated in the top panel of Figure [4]. A similar trend is observed when considering the X-ray luminosity (bottom panel of Figure [4]), with the break (L^*_{14-150}) in the LF[33] being consistent with the transition between an AGN being mostly obscured to being mostly unobscured. Most of the SMBH growth in the local universe should occur around the break in the LF (e.g.,
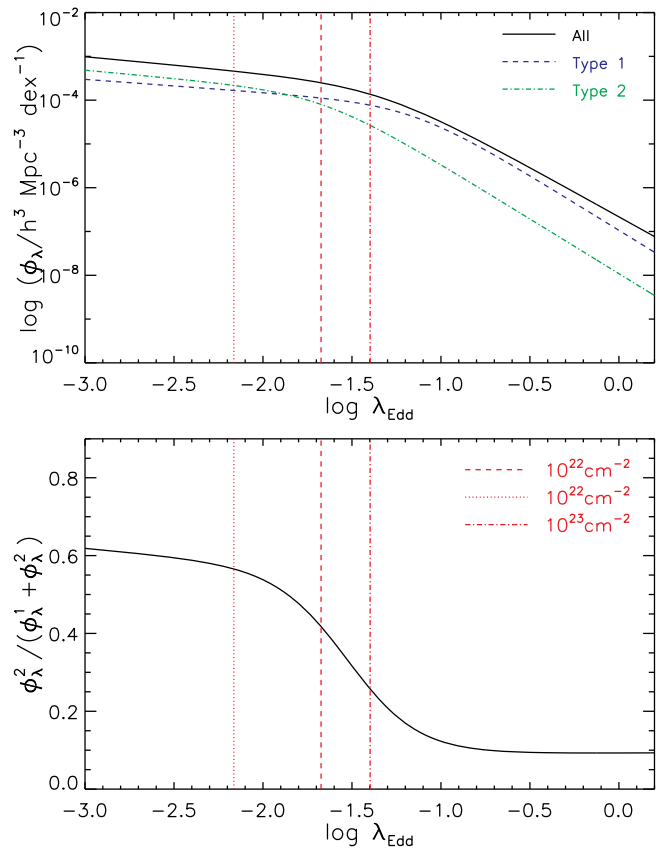
---

[33] Ananna et al. ([2022b]) report the luminosity in the 14–195 keV band, which was converted into the 14–150 keV luminosity adopted here assuming a power-law continuum with a photon index of $\Gamma = 1.8$, consistent with the median of Swift/BAT AGNs (Ricci et al. [2017b]).


Figure 3. Top panel: ERDFs of type 1 and type 2 BASS AGNs from Ananna et al. ([2022b]). The vertical red lines show the expected Eddington limit for dusty gas with $\log(N_{\rm H}/{\rm cm}^{-2}) \simeq 22$ (dashed line from Fabian et al. [2006], [2008], [2009]; dotted line from Ishibashi et al. [2018]) and $\log(N_{\rm H}/{\rm cm}^{-2}) \simeq 23$ (dotted–dashed line from Ishibashi et al. [2018]; see also Venanzi et al. [2020]). Bottom panel: ratio between the Eddington ratio distribution function of type 2 AGNs and that of the whole AGN population, which is a proxy of the fraction of obscured sources and of the covering factor of the obscuring material.

Hopkins et al. [2005]; Hopkins & Hernquist [2009]), which corresponds, for our sample of nearby AGNs, to the phase during which the accreting SMBH is surrounded by large quantities of gas and dust. Since the number density of AGNs strongly decreases at $\lambda_{\rm Edd} \gtrsim \lambda^*_{\rm Edd}$, this suggests that, in removing the obscuring material, radiation pressure from the AGN also depletes the reservoir of the fueling material, thus regulating accretion onto the SMBH, and causing the shorter lifetime of AGNs accreting at high Eddington ratios.

The differences in the Eddington ratio distributions of obscured and unobscured AGNs, as well as the overall shape of the ERDF and LF, can be interpreted in the framework of an evolutionary model, in which radiation pressure, besides shaping the close environment of SMBHs, also regulates their growth. A schematic of this radiation-regulated growth model of SMBHs, which is an extension of the radiation-regulated unification model (Ricci et al. [2017a]), is shown in Figure [5]: an accretion event (1) increases the Eddington ratio, typical column density, and covering factor of the circumnuclear obscuring material of an AGN (2). Due to the large covering factor of the circumnuclear obscuring material, an AGN in this stage would be preferentially observed as obscured by an observer at a random inclination angle. As the Eddington ratio increases due to the large amount of fuel available, the source eventually reaches the effective Eddington limit for dusty gas.
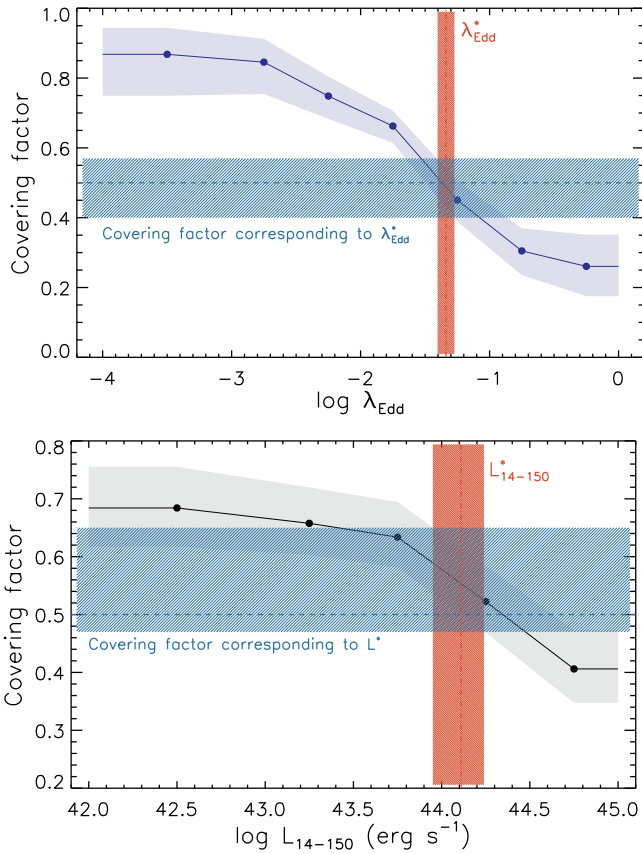
Figure 4. Top panel: covering factor of obscuring material vs. Eddington ratio for the objects in our hard X-ray selected sample with $-4 \leqslant \log \lambda_{\mathrm{Edd}} < 0$. The covering factor was obtained by considering the fraction of obscured sources, as in Figure 1, including the Compton-thick fraction from Ricci et al. (2017a), and normalizing to unity in the $20 \leqslant \log(N_{\mathrm{H}}/\mathrm{cm}^{-2}) < 25$ interval. The red vertical line shows the break in the ERDF (λ_{Edd}^*), while the hatched vertical area shows the uncertainty on λ_{Edd}^* (Ananna et al. 2022b). The blue hatched horizontal area represents the observed interval of the covering factor overlapping with λ_{Edd}^*. The blue dashed line corresponds to $f_{\mathrm{obs}} = 50\%$. The value of λ_{Edd}^* corresponds to the Eddington ratio where the transition between most of the sources being obscured ($f_{\mathrm{obs}} > 50\%$) to most of the sources being unobscured ($f_{\mathrm{obs}} < 50\%$) is observed. Bottom panel: same as the top panel for the 14–150 keV luminosity. The red vertical line shows the break in the LF (L_{14-150}^*), while the hatched vertical area shows its uncertainty (Ananna et al. 2022b).
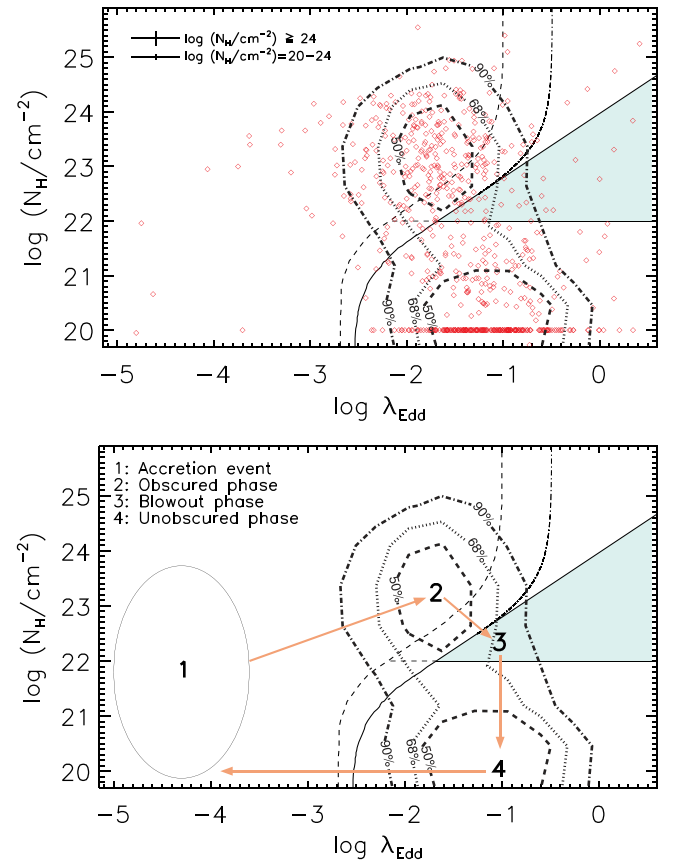
Figure 5. Top panel: BASS AGNs (red diamonds) in the N_{H}–λ_{Edd} plane. The dashed, dotted, and dotted–dashed black lines represent the 50%, 68%, and 90% number density contours in the $10^{-3} \leqslant \lambda_{\mathrm{Edd}} \leqslant 1$ range. The black continuous line represents the effective Eddington limit for dusty gas reported in Fabian et al. (2009). The horizontal line at $\log(N_{\mathrm{H}}/\mathrm{cm}^{-2}) = 22$ represents the assumed maximum contribution to N_{H} of gas from the host galaxy. The colored surface represents the blowout region. The dashed–dotted line shows the effective Eddington limit when including infrared radiation trapping (Ishibashi et al. 2018), adapted to the values of Fabian et al. (2009), similarly to what was done by Lansbury et al. (2020). The dashed line represents the effective Eddington limit for dusty gas reported by Ishibashi et al. (2018; see also Venanzi et al. 2020). The typical uncertainties are reported in the top-left corner for Compton-thin and CT AGNs. Sources for which N_{H} was too low to be constrained were assigned $\log(N_{\mathrm{H}}/\mathrm{cm}^{-2}) = 20$. The low number of low λ_{Edd} points is due to relatively low sensitivity of Swift/BAT, which does not allow it to detect low-luminosity AGNs. Bottom panel: a schematic of the radiation-regulated growth model outlined here: an accretion event (1) leads to an increase of the Eddington ratio and typical column density of an AGN (2), which would be preferentially observed as an obscured or type 2 source, due to the large covering factor of the obscuring material. As the Eddington ratio increases above the effective Eddington limit for dusty gas, the AGN spends a short time in the blowout region (3), before its covering factor decreases, and it is mostly observed as an unobscured or type 1 source (4). Once most of the material has been accreted, or blown away by infrared radiation trapping, the source moves back to having low values of N_{H} and λ_{Edd}. The lines are the same as in the top panel.

It then spends a short time in the blowout region (3), with the covering factor of the circumnuclear obscuring material decreasing rapidly, until most of the circumnuclear obscuring material is blown away, and the AGN is more likely observed as a relatively unobscured source (4). This would leave mostly optically thick material located near the plane of the disk, in agreement with the finding that the covering factor of the CT gas does not change significantly with Eddington ratio (Ricci et al. 2017a). Once most of the material has been accreted and/ or has been blown away by radiation pressure and IR trapping, the source would transition to low N_{H} and λ_{Edd}.

The timescales of this process will be discussed in detail, using the ERDF, in a forthcoming companion paper (Ananna et al. 2022a; see also Lansbury et al. 2020 and Jun et al. 2021 for a recent discussion on the blowout timescales). It should be noted that in Figure 5 we assumed a maximum contribution of the host galaxy to the X-ray obscuration of $\log(N_{\mathrm{H}}/\mathrm{cm}^{-2}) \sim 22$, i.e., ~ 1 dex higher than the angle-averaged value obtained for the Milky Way (e.g., Willingale

et al. 2013), although this value could be larger for high stellar masses (e.g., Buchner et al. 2017) and could increase significantly at higher redshifts (e.g., Banerji et al. 2012; Assef et al. 2015; LaMassa et al. 2016; Gilli et al. 2022; see Section 4.3). The accretion event could be either associated with secular processes (e.g., Davies et al. 2007) or with mergers (e.g., Blecha et al. 2018). Both mechanisms could be at play in our AGN population: Swift/BAT AGNs tend to be hosted by gas-rich spiral galaxies (e.g., Koss et al. 2011) and to have high gas fractions (Koss et al. 2021), and some of them can be found in galaxy mergers (e.g., Koss et al. 2018).

According to the model proposed here, the obscuring material of objects at the end of the cycle, with low Eddington ratios ($\log \lambda_{\mathrm{Edd}} \lesssim -4$), would be expected to have lower covering factor and column density. While the statistics available are still small, this could be reflected in the lower fraction of obscured sources observed in the $-4.8 \leqslant \log \lambda_{\mathrm{Edd}} \leqslant -4$ range (Ricci et al. 2017a, Figure 1). These very low Eddington ratio AGNs typically show only faint X-ray reflection features (e.g., Ptak et al. 2004), and recent modeling of their broadband X-ray spectra has also shown that their integrated column densities appear to be significantly lower than those of more rapidly accreting SMBHs (e.g., Ursini et al. 2015; Diaz et al. 2020). This might not be the case for all low λ_{Edd} AGNs, since some of them might be in the process of starting a new cycle (i.e., transitioning from step 1 to 2 in Figure 5). Low-luminosity AGNs (e.g., Ho 2008, 2009) are still expected to produce feedback, preferentially through the kinetic mode (e.g., Weinberger et al. 2017), which would however mostly heat up the gas on Galactic scales, and not strongly affect the circumnuclear environment of the SMBH.

4.3. The Role of Large-scale Obscuration at High Redshift

At higher redshifts and luminosities than those probed here, it seems to be rather common for sources accreting at very high λ_{Edd} to be obscured. This is shown, for example, by the relatively high number density of hot dust obscured galaxies (hot DOGs), which are found to have large $[\log(N_{\mathrm{H}}/\mathrm{cm}^{-2}) > 23]$ column densities (e.g., Stern et al. 2014; Ricci et al. 2017c; Vito et al. 2018a; Zappacosta et al. 2018b) compared to AGNs with similar luminosities (Assef et al. 2015). Red quasars, which host obscured AGNs (e.g., Banerji et al. 2012; LaMassa et al. 2016; Glikman et al. 2017), have also been found to reside in the blowout region of the $N_{\mathrm{H}}-\lambda_{\mathrm{Edd}}$ diagram (Glikman 2017; Lansbury et al. 2020). Moreover, many of these objects show evidence of powerful outflows in their optical/UV spectra (e.g., Yi et al. 2022), suggesting they are in the process of driving material away from the nucleus (Temple et al. 2019; Lansbury et al. 2020). Jun et al. (2021) recently studied a large sample of infrared and submillimeter-bright obscured quasars with bolometric luminosities $L_{\mathrm{Bol}} \gtrsim 10^{46}\,\mathrm{erg\,s}^{-1}$, which included red quasars, Hot DOGs, ultraluminous infrared galaxies, and submillimeter galaxies. Jun et al. (2021) showed that most of these objects are found in the blowout region, and behave differently from lower-luminosity, local AGNs. In some of these objects, the AGN might be in the brief phase during which it is expelling dusty circumnuclear gas, and cleaning up its environment. This behavior in IR-bright and submillimeter galaxies could also be related to the high fraction of mergers found in these objects (e.g., Urrutia et al. 2008; Glikman et al. 2015; Fan et al. 2016; Díaz-Santos et al. 2018). Theoretical studies have shown that the merger process can be very efficient in moving gas into the inner hundreds of parsecs of galaxies, thus feeding and obscuring the SMBH (e.g., Hopkins et al. 2008; Blecha et al. 2018; Kawaguchi et al. 2020). In agreement with this, it has been found that the typical column density and covering factor of the obscuring material is very high in galaxies undergoing mergers, particularly during the final stages (Ricci et al. 2017d, 2021; see also Satyapal et al. 2014; Kocevski et al. 2015; Yamada et al. 2021). Part of this material could be located outside the sphere of influence of the SMBH, so that the main parameter determining the effect of radiation pressure would be the luminosity, rather than the Eddington ratio. Moreover, it has

been argued that the presence of stars in the dusty gas clouds would hinder the effect of radiation pressure (Fabian et al. 2009), since they would provide an additional gravitational pull, allowing the obscuring material to survive to higher λ_{Edd}. Therefore, in the case of major merger-induced accretion, the radiation-regulated growth model illustrated in Figure 5 could reach higher column densities (e.g., Ricci et al. 2017d, 2021) and accretion rates (e.g., Treister et al. 2012).

The ISM could also play a role in obscuring the AGN at redshifts higher than those probed by our study. Using ALMA observations, Gilli et al. (2022) recently showed that the column density of the ISM toward the nucleus of $z > 3$ galaxies is typically >100 times larger than at $z \sim 0$, and it may reach CT values at $z \gtrsim 6$. This, combined with the larger number of AGNs in mergers at higher redshifts with respect to $z \simeq 0$ (e.g., Mortlock et al. 2013; Whitney et al. 2021), could explain the increase of the fraction of obscured sources with redshift (e.g., La Franca et al. 2005; Treister & Urry 2006; Ueda et al. 2014; Aird et al. 2015; Buchner et al. 2015; Vito et al. 2018b; Avirett-Mackenzie & Ballantyne 2019), and in particular the high fraction of AGNs with $\log(N_{\mathrm{H}}/\mathrm{cm}^{-2}) \gtrsim 23$ at $z > 3$ (Vito et al. 2018b). Since the ISM material is outside the sphere of influence of the SMBH, in these high-z objects, the relation between radiative AGN feedback and the obscuring material would be regulated by luminosity, and not by Eddington ratio. This would allow AGNs to reach higher luminosities before they are able to remove the obscuring gas. If part of the obscuring material is associated with the AGN feeding, one would expect the break in the ERDF to shift to higher values for higher redshifts (e.g., Caplar et al. 2015; Schulze et al. 2015), similarly to what is observed for the break in the LF (e.g., Ueda et al. 2014).

5. Summary and Conclusions

We studied here the relation between AGN obscuration and the Eddington ratio using a highly complete sample of 681 nearby X-ray selected AGNs with black hole mass measurements from BASS, with the goal of improving our understanding of the relation between obscuration, radiation pressure, and SMBH growth. Our main findings are:

1. Thanks to the significantly larger sample, we confirm with a higher statistical significance the results obtained by Ricci et al. (2017a), namely that the fraction of obscured sources decreases sharply at $\lambda_{\mathrm{Edd}} \gtrsim 10^{-2}$ (Figure 1), corresponding to the Eddington limit for dusty gas (Fabian et al. 2006, 2008, 2009). This suggests that radiative feedback can efficiently remove the obscuring material around SMBHs.

2. Using the large BASS data set, we find a strong increase in the fraction of sources with $\log(N_{\mathrm{H}}/\mathrm{cm}^{-2}) < 21$ at $\lambda_{\mathrm{Edd}} \gtrsim 10^{-2}$, consistent with the idea that obscured sources become fully unobscured rapidly once they accrete above the effective Eddington limit for dusty gas (top-left panel of Figure 2).

3. The fraction of sources with $21 \leqslant \log(N_{\mathrm{H}}/\mathrm{cm}^{-2}) < 22$ does not change with λ_{Edd}, and is stable at $\sim 15\%$–20%, suggesting that most of the (neutral or weakly ionized) obscuration in these AGNs is produced by gas in their host galaxies (top-right panel of Figure 2).

4. The fraction of sources with $22 \leqslant \log(N_{\mathrm{H}}/\mathrm{cm}^{-2}) < 23$ decreases rapidly at $\lambda_{\mathrm{Edd}} \gtrsim 10^{-2}$ (bottom-left panel of

Figure 2), consistent with the radiation-regulated unification model (Ricci et al. 2017a). Interestingly, the fraction of sources with $23 \leqslant \log(N_H/\mathrm{cm}^{-2}) < 24$ also decreases at a similar Eddington ratio (bottom-right panel of Figure 2). This could be due to the effect of infrared radiation trapping (e.g., Ishibashi et al. 2018; Venanzi et al. 2020), which is expected to lead material with $\log(N_H/\mathrm{cm}^{-2}) \gtrsim 23$ to evaporate at λ_{Edd} below the expected Eddington limit for dusty gas with the same column density.

5. Using the ratio between the ERDF of type 2 AGNs and the ERDF of type 1 and type 2 AGNs (Ananna et al. 2022b), we recover a similar relation between the covering factor and the Eddington ratio to that found using the fraction of obscured sources (Figure 3; see also Ricci et al. 2017a).

6. The breaks in the ERDF ($\log \lambda_{Edd}^* = -1.34 \pm 0.07$) and LF ($\log L_{14-150}^* = 44.11_{-0.16}^{+0.13}$) of all BAT AGNs (Ananna et al. 2022b) are found where AGNs transition from having most of their sky covered by obscuring material to having most of their sky devoid of absorbing material (Figure 4). This implies that most of the SMBH growth in the local universe would happen when an AGN is covered by a large fraction of gas and dust. The fact that AGNs with Eddington ratios above λ_{Edd}^*, which have low covering factors of the obscuring material, are rarer, could be associated with the lower amount of accreting material available in their surroundings, which would lead them to spend a relatively short time in this phase.

7. We suggest that these results could be explained with a radiation-regulated growth model for AGNs (see Figure 5), in which (nearby) accreting SMBHs move in the $N_H-\lambda_{Edd}$ plane during their life cycle. The growth episode starts with the AGN mostly unobscured and accreting at low λ_{Edd}. As the SMBH receives its fuel, its λ_{Edd}, N_H, and covering factor increase. At this stage, an observer, with a randomly selected inclination angle with respect to the obscuring material, would preferentially observe the source as an obscured/type 2 AGN. When λ_{Edd} increases above the Eddington limit for dusty gas, the AGN starts to rapidly expel the obscuring material, which leads to a rapid decrease of its covering factor and typical N_H. The AGN is now observed typically as unobscured/type 1, with only CT material along the equatorial plane left. As the material is depleted, either by accretion or by the effect of infrared radiation trapping due to the increasing λ_{Edd}, the SMBH goes back to a quiescent phase.

In a parallel and complementary BASS analysis (Ananna et al. 2022a), we will use the ERDF of nearby AGNs to constrain the timescales of the different stages of SMBH growth. At redshifts higher than those probed here, large-scale material associated with the host galaxy might play an important role in obscuring AGNs (e.g., Gilli et al. 2022), and the main parameter determining the effect of radiation pressure could be the luminosity, rather than the Eddington ratio. Future studies of the redshift evolution of the $f_{obs}-\lambda_{Edd}$ relation, and evolution of the $N_H-\lambda_{Edd}$ diagram, will help shed light on how the relation between AGN obscuration and radiative feedback changes over cosmic time.

Appendix
The Effect of Black Hole Mass and Luminosity on the Obscuration–Eddington Ratio Relation

In the top and bottom panels of Figure 6, we show the relation between the fraction of sources with given column density and the Eddington ratio. The sources are divided into two different ranges of 14–150 keV intrinsic luminosity (top panels) and black hole mass (bottom panels), showing that these two parameters do not play a significant role.
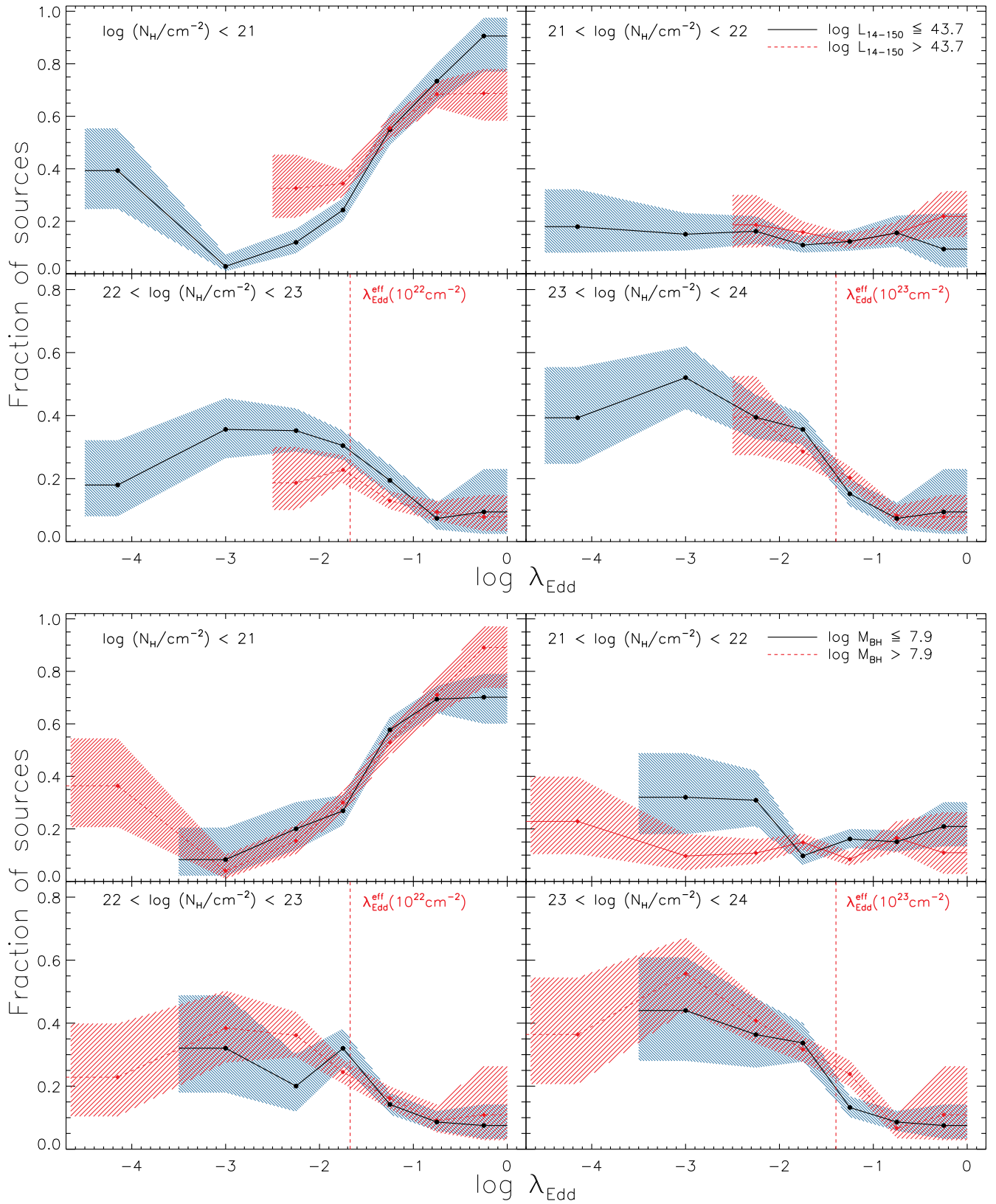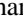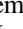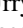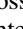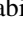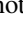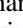
Figure 6. Top panel: fraction of sources with column densities in a given range vs. the Eddington ratio for AGNs in two different bins o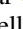f intrinsic 14–150 keV luminosity (in units of erg s^{-1}). The red dashed lines show the expected Eddington limit for dusty gas with $\log(N_H/cm^{-2}) \simeq 22$ (bottom-left panel; Fabian et al. 2006, 2008, 2009) and $\log(N_H/cm^{-2}) \simeq 23$ (bottom-right panel; Ishibashi et al. 2018; Venanzi et al. 2020). The latter value of the effective Eddington limit includes the contribution from IR radiation trapping. Bottom panel: same as top panel, but with AGNs divided into two different ranges of black hole mass (in units of solar mass).

ORCID iDs

C. Ricci ⑩ https://orcid.org/0000-0001-5231-2645
T. T. Ananna ⑩ https://orcid.org/0000-0001-8211-3807
M. J. Temple ⑩ https://orcid.org/0000-0001-8433-550X
C. M. Urry ⑩ https://orcid.org/0000-0002-0745-9792
M. J. Koss ⑩ https://orcid.org/0000-0002-7998-9581
B. Trakhtenbrot ⑩ https://orcid.org/0000-0002-3683-7297
Y. Ueda ⑩ https://orcid.org/0000-0001-7821-6715
D. Stern ⑩ https://orcid.org/0000-0003-2686-9241
F. E. Bauer ⑩ https://orcid.org/0000-0002-8686-8737
E. Treister ⑩ https://orcid.org/0000-0001-7568-6412
G. C. Privon ⑩ https://orcid.org/0000-0003-3474-1125
K. Oh ⑩ https://orcid.org/0000-0002-5037-951X
M. Stalevski ⑩ https://orcid.org/0000-0001-5146-8330
L. C. Ho ⑩ https://orcid.org/0000-0001-6947-5846
A. C. Fabian ⑩ https://orcid.org/0000-0002-9378-4072
R. Mushotzky ⑩ https://orcid.org/0000-0002-7962-5446
C. S. Chang ⑩ https://orcid.org/0000-0001-9910-3234
L. Sartori ⑩ https://orcid.org/0000-0001-8020-3884
R. Baer ⑩ https://orcid.org/0000-0001-5481-8607
T. Caglar ⑩ https://orcid.org/0000-0002-9144-2255
M. Powell ⑩ https://orcid.org/0000-0003-2284-8603

References

Aird, J., Coil, A. L., Georgakakis, A., et al. 2015, MNRAS, 451, 1892
Aird, J., Coil, A. L., & Georgakakis, A. 2018, MNRAS, 474, 1225
Aird, J., Coil, A. L., Moustakas, J., et al. 2012, ApJ, 746, 90
Aird, J., Nandra, K., Laird, E. S., et al. 2010, MNRAS, 401, 2531
Akylas, A., Georgantopoulos, I., Ranalli, P., et al. 2016, A&A, 594, A73
Alexander, D. M., Stern, D., Del Moro, A., et al. 2013, ApJ, 773, 125
Alonso-Herrero, A., García-Burillo, S., Hönig, S. F., et al. 2021, A&A, 652, A99
Ananna, T. T., Treister, E., Urry, C. M., et al. 2019, ApJ, 871, 240
Ananna, T. T., Urry, C. M., Ricci, C., et al. 2022a, ApJ, submitted
Ananna, T. T., Weigel, A. K., Trakhtenbrot, B., et al. 2022b, ApJS, 261, 9
Antonucci, R. 1993, ARA&A, 31, 473
Asmus, D. 2019, MNRAS, 489, 2177
Assef, R. J., Eisenhardt, P. R. M., Stern, D., et al. 2015, ApJ, 804, 27
Avirett-Mackenzie, M. S., & Ballantyne, D. R. 2019, MNRAS, 486, 3488
Baek, J., Chung, A., Schawinski, K., et al. 2019, MNRAS, 488, 4317
Banerji, M., McMahon, R. G., Hewett, P. C., et al. 2012, MNRAS, 427, 2275
Barger, A. J., Cowie, L. L., Mushotzky, R. F., et al. 2005, AJ, 129, 578
Barthelmy, S. D., Barbier, L. M., Cummings, J. R., et al. 2005, SSRv, 120, 143
Baumgartner, W. H., Tueller, J., Markwardt, C. B., et al. 2013, ApJS, 207, 19
Beckmann, V., Soldi, S., Ricci, C., et al. 2009, A&A, 505, 417
Blecha, L., Snyder, G. F., Satyapal, S., & Ellison, S. L. 2018, MNRAS, 478, 3056
Bongiorno, A., Schulze, A., Merloni, A., et al. 2016, A&A, 588, A78
Bower, R. G., Benson, A. J., Malbon, R., et al. 2006, MNRAS, 370, 645
Brusa, M., Civano, F., Comastri, A., et al. 2010, ApJ, 716, 348
Buchner, J., Georgakakis, A., Nandra, K., et al. 2015, ApJ, 802, 89
Buchner, J., Schulze, S., & Bauer, F. E. 2017, MNRAS, 464, 4545
Burlon, D., Ajello, M., Greiner, J., et al. 2011, ApJ, 728, 58
Cameron, E. 2011, PASA, 28, 128
Caplar, N., Lilly, S. J., & Trakhtenbrot, B. 2015, ApJ, 811, 148
Caputi, K. I., Lagache, G., Yan, L., et al. 2007, ApJ, 660, 97
Civano, F., Hickox, R. C., Puccetti, S., et al. 2015, ApJ, 808, 185
Croton, D. J., Springel, V., White, S. D. M., et al. 2006, MNRAS, 365, 11
Cusumano, G., La Parola, V., Segreto, A., et al. 2010, A&A, 524, A64
Davies, R. I., Müller Sánchez, F., Genzel, R., et al. 2007, ApJ, 671, 1388
Del Moro, A., Alexander, D. M., Aird, J. A., et al. 2017, ApJ, 849, 57
Della Ceca, R., Caccianiga, A., Severgnini, P., et al. 2008, A&A, 487, 119
den Brok, J. S., Koss, M. J., Trakhtenbrot, B., et al. 2022, ApJS, 261, 7
Diaz, Y., Arévalo, P., Hernández-García, L., et al. 2020, MNRAS, 496, 5399
Díaz-Santos, T., Assef, R. J., Blain, A. W., et al. 2018, Sci, 362, 1034
Elvis, M., Wilkes, B. J., McDowell, J. C., et al. 1994, ApJS, 95, 1
Ezhikode, S. H., Gandhi, P., Done, C., et al. 2017, MNRAS, 472, 3492
Fabian, A. C. 2012, ARA&A, 50, 455
Fabian, A. C., Celotti, A., & Erlund, M. C. 2006, MNRAS, 373, L16

Fabian, A. C., Vasudevan, R. V., & Gandhi, P. 2008, MNRAS, 385, L43
Fabian, A. C., Vasudevan, R. V., Mushotzky, R. F., Winter, L. M., & Reynolds, C. S. 2009, MNRAS, 394, L89
Fan, L., Han, Y., Fang, G., et al. 2016, ApJ, 822, L32
Ferrarese, L., & Merritt, D. 2000, ApJ, 539, L9
García-Burillo, S., Alonso-Herrero, A., Ramos Almeida, C., et al. 2021, A&A, 652, A98
Gebhardt, K., Bender, R., Bower, G., et al. 2000, ApJ, 539, L13
Gehrels, N., Chincarini, G., Giommi, P., et al. 2004, ApJ, 611, 1005
Georgakakis, A., Aird, J., Schulze, A., et al. 2017, MNRAS, 471, 1976
Gilli, R., Norman, C., Calura, F., et al. 2022, arXiv:2206.03508
Glikman, E. 2017, RNAAS, 1, 48
Glikman, E., LaMassa, S., Piconcelli, E., Urry, M., & Lacy, M. 2017, ApJ, 847, 116
Glikman, E., Simmons, B., Mailly, M., et al. 2015, ApJ, 806, 218
Greene, J. E., & Ho, L. C. 2007, ApJ, 667, 131
Häring, N., & Rix, H.-W. 2004, ApJ, 604, L89
Harrison, F. A., Aird, J., Civano, F., et al. 2016, ApJ, 831, 185
Hasinger, G. 2008, A&A, 490, 905
Hickox, R. C., & Alexander, D. M. 2018, ARA&A, 56, 625
Ho, L. C. 2008, ARA&A, 46, 475
Ho, L. C. 2009, ApJ, 699, 626
Hönig, S. F., & Beckert, T. 2007, MNRAS, 380, 1172
Hönig, S. F., & Kishimoto, M. 2017, ApJ, 838, L20
Hönig, S. F., Kishimoto, M., Tristram, K. R. W., et al. 2013, ApJ, 771, 87
Hopkins, P. F., & Hernquist, L. 2009, ApJ, 698, 1550
Hopkins, P. F., Hernquist, L., Cox, T. J., et al. 2005, ApJ, 630, 716
Hopkins, P. F., Hernquist, L., Cox, T. J., & Kereš, D. 2008, ApJS, 175, 356
Hopkins, P. F., Richards, G. T., & Hernquist, L. 2007, ApJ, 654, 731
Ichikawa, K., Ricci, C., Ueda, Y., et al. 2017, ApJ, 835, 74
Ichikawa, K., Ricci, C., Ueda, Y., et al. 2019, ApJ, 870, 31
Ishibashi, W., Fabian, A. C., Ricci, C., & Celotti, A. 2018, MNRAS, 479, 3335
Jun, H. D., Assef, R. J., Carroll, C. M., et al. 2021, ApJ, 906, 21
Kakkad, D., Sani, E., Rojas, A. F., et al. 2022, MNRAS, 511, 2105
Kawaguchi, T., & Mori, M. 2010, ApJ, 724, L183
Kawaguchi, T., Yutani, N., & Wada, K. 2020, ApJ, 890, 125
Kawakatu, N., Wada, K., & Ichikawa, K. 2020, ApJ, 889, 84
Kawamuro, T., Ricci, C., Imanishi, M., et al. 2022, arXiv:2208.03880
Kelly, B. C., & Shen, Y. 2013, ApJ, 764, 45
Kocevski, D. D., Brightman, M., Nandra, K., et al. 2015, ApJ, 814, 104
Kollmeier, J. A., Onken, C. A., Kochanek, C. S., et al. 2006, ApJ, 648, 128
Kormendy, J., & Ho, L. C. 2013, ARA&A, 51, 511
Kormendy, J., & Richstone, D. 1995, ARA&A, 33, 581
Koss, M., Mushotzky, R., Treister, E., et al. 2012, ApJ, 746, L22
Koss, M., Mushotzky, R., Veilleux, S., et al. 2011, ApJ, 739, 57
Koss, M., Trakhtenbrot, B., Ricci, C., et al. 2017, ApJ, 850, 74
Koss, M. J., Blecha, L., Bernhard, P., et al. 2018, Nature, 563, 214
Koss, M. J., Ricci, C., Trakhtenbrot, B., et al. 2022b, ApJS, 261, 2
Koss, M. J., Strittmatter, B., Lamperti, I., et al. 2021, ApJS, 252, 29
Koss, M. J., Trakhtenbrot, B., Ricci, C., et al. 2022a, ApJS, 261, 1
Koss, M. J., Trakhtenbrot, B., Ricci, C., et al. 2022c, ApJS, 261, 6
Krivonos, R. A., Sazonov, S. Y., Kuznetsova, E. A., et al. 2022, MNRAS, 510, 4796
La Franca, F., Fiore, F., Comastri, A., et al. 2005, ApJ, 635, 864
LaMassa, S. M., Ricarte, A., Glikman, E., et al. 2016, ApJ, 820, 70
Lamperti, I., Koss, M., Trakhtenbrot, B., et al. 2017, MNRAS, 467, 540
Lansbury, G. B., Banerji, M., Fabian, A. C., & Temple, M. J. 2020, MNRAS, 495, 2652
Lanz, L., Hickox, R. C., Baloković, M., et al. 2019, ApJ, 870, 26
Lawrence, A. 1991, MNRAS, 252, 586
Lawrence, A., & Elvis, M. 1982, ApJ, 256, 410
López-Gonzaga, N., Burtscher, L., Tristram, K. R. W., Meisenheimer, K., & Schartmann, M. 2016, A&A, 591, A47
Lusso, E., Hennawi, J. F., Comastri, A., et al. 2013, ApJ, 777, 86
Maiolino, R., Shemmer, O., Imanishi, M., et al. 2007, A&A, 468, 979
Malizia, A., Bassani, L., Stephen, J. B., Bazzano, A., & Ubertini, P. 2020, A&A, 639, A5
Marchesi, S., Ajello, M., Marcotulli, L., et al. 2018, ApJ, 854, 49
Marconi, A., & Hunt, L. K. 2003, ApJ, 589, L21
Markwardt, C. B., Tueller, J., Skinner, G. K., et al. 2005, ApJ, 633, L77
Masini, A., Civano, F., Comastri, A., et al. 2018, ApJS, 235, 17
Mateos, S., Carrera, F. J., Barcons, X., et al. 2017, ApJ, 841, L18
Mejía-Restrepo, J. E., Trakhtenbrot, B., Koss, M. J., et al. 2022, ApJS, 261, 5
Mortlock, A., Conselice, C. J., Hartley, W. G., et al. 2013, MNRAS, 433, 1185
Mullaney, J. R., Del-Moro, A., Aird, J., et al. 2015, ApJ, 808, 184
Nagar, N. M., Falcke, H., & Wilson, A. S. 2005, A&A, 435, 521

Netzer, H. 2015, ARA&A, 53, 365
Netzer, H., Lani, C., Nordon, R., et al. 2016, ApJ, 819, 123
Ogawa, S., Ueda, Y., Tanimoto, A., & Yamada, S. 2021, ApJ, 906, 84
Oh, K., Koss, M., Markwardt, C. B., et al. 2018, ApJS, 235, 4
Oh, K., Schawinski, K., Koss, M., et al. 2017, MNRAS, 464, 1466
Oh, K., Yi, S. K., Schawinski, K., et al. 2015, ApJS, 219, 1
Paliya, V. S., Koss, M., Trakhtenbrot, B., et al. 2019, ApJ, 881, 154
Paltani, S., Walter, R., McHardy, I. M., et al. 2008, A&A, 485, 707
Ptak, A., Terashima, Y., Ho, L. C., & Quataert, E. 2004, ApJ, 606, 173
Ramos Almeida, C., & Ricci, C. 2017, NatAs, 1, 679
Ricci, C., Assef, R. J., Stern, D., et al. 2017c, ApJ, 835, 105
Ricci, C., Bauer, F. E., Treister, E., et al. 2017d, MNRAS, 468, 1273
Ricci, C., Beckmann, V., Audard, M., & Courvoisier, T. J. L. 2010, A&A,
    518, A47
Ricci, C., Ho, L. C., Fabian, A. C., et al. 2018, MNRAS, 480, 1819
Ricci, C., Privon, G. C., Pfeifle, R. W., et al. 2021, MNRAS, 506, 5935
Ricci, C., Trakhtenbrot, B., Koss, M. J., et al. 2017a, Nature, 549, 488
Ricci, C., Trakhtenbrot, B., Koss, M. J., et al. 2017b, ApJS, 233, 17
Ricci, C., Ueda, Y., Koss, M. J., et al. 2015, ApJ, 815, L13
Ricci, F., Treister, E., Bauer, F. E., et al. 2022, ApJS, 261, 8
Rojas, A. F., Sani, E., Gavignaud, I., et al. 2020, MNRAS, 491, 5867
Ross, N. P., McGreer, I. D., White, M., et al. 2013, ApJ, 773, 14
Satyapal, S., Ellison, S. L., McAlpine, W., et al. 2014, MNRAS, 441, 1297
Sazonov, S., Willner, S. P., Goulding, A. D., et al. 2012, ApJ, 757, 181
Schaye, J., Crain, R. A., Bower, R. G., et al. 2015, MNRAS, 446, 521
Schulze, A., Bongiorno, A., Gavignaud, I., et al. 2015, MNRAS, 447, 2085
Schulze, A., & Wisotzki, L. 2010, A&A, 516, A87
Shankar, F., Salucci, P., Granato, G. L., De Zotti, G., & Danese, L. 2004,
    MNRAS, 354, 1020
She, R., Ho, L. C., Feng, H., & Cui, C. 2018, ApJ, 859, 152
Sijacki, D., Springel, V., Di Matteo, T., & Hernquist, L. 2007, MNRAS,
    380, 877
Simpson, C. 2005, MNRAS, 360, 565
Smith, K. L., Mushotzky, R. F., Koss, M., et al. 2020, MNRAS, 492, 4216
Soltan, A. 1982, MNRAS, 200, 115
Stalevski, M., Ricci, C., Ueda, Y., et al. 2016, MNRAS, 458, 2288
Steffen, A. T., Barger, A. J., Cowie, L. L., Mushotzky, R. F., & Yang, Y. 2003,
    ApJ, 596, L23
Stern, D., Lansbury, G. B., Assef, R. J., et al. 2014, ApJ, 794, 102
Tanimoto, A., Ueda, Y., Odaka, H., Yamada, S., & Ricci, C. 2022, ApJS,
    260, 30
Temple, M. J., Banerji, M., Hewett, P. C., et al. 2019, MNRAS, 487, 2594
Toba, Y., Ueda, Y., Gandhi, P., et al. 2021, ApJ, 912, 91
Torres-Albà, N., Marchesi, S., Zhao, X., et al. 2021, ApJ, 922, 252
Trakhtenbrot, B., Ricci, C., Koss, M. J., et al. 2017, MNRAS, 470, 800
Treister, E., Krolik, J. H., & Dullemond, C. 2008, ApJ, 679, 140
Treister, E., Schawinski, K., Urry, C. M., & Simmons, B. D. 2012, ApJ,
    758, L39
Treister, E., & Urry, C. M. 2006, ApJ, 652, L79
Tristram, K. R. W., Meisenheimer, K., Jaffe, W., et al. 2007, A&A, 474, 837
Tueller, J., Baumgartner, W. H., Markwardt, C. B., et al. 2010, ApJS, 186, 378
Tueller, J., Mushotzky, R. F., Barthelmy, S., et al. 2008, ApJ, 681, 113
Ueda, Y., Akiyama, M., Hasinger, G., Miyaji, T., & Watson, M. G. 2014, ApJ,
    786, 104
Ueda, Y., Akiyama, M., Ohta, K., & Miyaji, T. 2003, ApJ, 598, 886
Urrutia, T., Lacy, M., & Becker, R. H. 2008, ApJ, 674, 80
Urry, C. M., & Padovani, P. 1995, PASP, 107, 803
Ursini, F., Marinucci, A., Matt, G., et al. 2015, MNRAS, 452, 3266
Venanzi, M., Hönig, S., & Williamson, D. 2020, ApJ, 900, 174
Vito, F., Brandt, W. N., Stern, D., et al. 2018a, MNRAS, 474, 4528
Vito, F., Brandt, W. N., Yang, G., et al. 2018b, MNRAS, 473, 2378
Weigel, A. K., Schawinski, K., Caplar, N., et al. 2017, ApJ, 845, 134
Weinberger, R., Springel, V., Hernquist, L., et al. 2017, MNRAS, 465, 3291
Whitney, A., Ferreira, L., Conselice, C. J., & Duncan, K. 2021, ApJ, 919, 139
Willingale, R., Starling, R. L. C., Beardmore, A. P., Tanvir, N. R., &
    O'Brien, P. T. 2013, MNRAS, 431, 394
Winter, L. M., Mushotzky, R. F., Reynolds, C. S., & Tueller, J. 2009, ApJ,
    690, 1322
Yamada, S., Ueda, Y., Tanimoto, A., et al. 2021, ApJS, 257, 61
Yi, W., Brandt, W. N., Ni, Q., et al. 2022, ApJ, 930, 5
Yu, Q., & Tremaine, S. 2002, MNRAS, 335, 965
Zappacosta, L., Comastri, A., Civano, F., et al. 2018a, ApJ, 854, 33
Zappacosta, L., Piconcelli, E., Duras, F., et al. 2018b, A&A, 618, A28
Zhao, X., Marchesi, S., Ajello, M., Baloković, M., & Fischer, T. 2020, ApJ,
    894, 71
Zhuang, M.-Y., Ho, L. C., & Shangguan, J. 2018, ApJ, 862, 118